Surface phonons of Ge(001) and their correlation with the $p(2 \times 1)$ and $c(4 \times 2)$ reconstruction as shown by Raman spectroscopy

Jochen Räthel, Eugen Speiser,[*] and Norbert Esser

Leibniz-Institut für Analytische Wissenschaften - ISAS - e.V., Albert-Einstein-Strasse 9, 12489 Berlin, Germany

Utz Bass, Sebastian Meyer, Jörg Schäfer, and Jean Geurts

Universität Würzburg, Physikalisches Institut, Am Hubland, 97074 Würzburg, Germany

The $p(2 \times 1)/c(4 \times 2)$ and the $c(4 \times 2)$ reconstruction of the Ge(001) surface have been studied by polarized Raman spectroscopy at 300 and 40 K, respectively. Raman spectra show several well-defined surface phonon modes related to the atomic structure of the Ge surface. Four modes are detected in the range between 5.70 and 28.15 meV. Their eigenenergies and polarization dependence agree with reported calculation results from the adiabatic bond charge model and from density-functional perturbation theory. The temperature-induced phase transition between both reconstructions is reflected in the symmetry selection rules. Moreover, our results reveal that in Raman scattering the impact of the well-known flipping of the buckled dimers in the $p(2 \times 1)$ reconstruction is fundamentally different from the time averaging, which occurs for low-energy electron diffraction (LEED) and scanning tunneling microscopy (STM). Since the phonon time scale is several orders of magnitude faster than the dimer flipping, the phonon oscillations and their Raman scattering are described consistently within the framework of quasistatic buckled dimers with a short-range antiferromagnetic in-row buckling order.

PACS number(s): 78.30.Am, 68.47.Fg, 68.35.B−, 68.35.Ja

I. INTRODUCTION

Besides Si(001), the Ge(001) surface is one of the most intensely studied semiconductor surfaces in the last decades. The widespread interest for this surface is essentially motivated by the simultaneous occurrence of a strong short-range interaction and a weak long-range interaction, giving rise to many interesting phenomena in its temperature-dependent reconstruction.[1] Additionally, this surface is employed as substrate for self-organized ordered atom assemblies in the monolayer range, which may exhibit pronounced electron-electron correlation phenomena, such as the recently evidenced Tomonaga-Luttinger liquid behavior of Au-induced one-dimensional chains on Ge(001).[2]

The basic step for the clean Ge(001) surface reconstruction is the formation of asymmetric [110]-directed dimers, which line up to rows along the [1$\bar{1}$0] direction,[3] while the higher order is induced by the in-row and row-to-row dimer buckling configuration. The top view on the reconstructions and the corresponding unit cells are shown in Fig. 1. For the clean Ge(001) surface three possible surface reconstructions have been proposed: $p(2 \times 1)$, $p(2 \times 2)$, and $c(4 \times 2)$, which were confirmed experimentally by real-space observation with STM.[1,3–5] Reciprocal space studies with LEED[6,7] and He diffraction[8] provide evidence only for the $p(2 \times 1)$ and $c(4 \times 2)$. A coexistence of the $p(2 \times 1)$ and $c(4 \times 2)$ in striped domains at room temperature was found in STM investigations.[1,4,5] The $p(2 \times 1)$ reconstruction in STM and LEED is explained as a continuous flip-flop between the two possible buckling orientation configurations, leading to a symmetric appearance as a time average.[5] Further systematic studies were performed by x-ray diffraction (XRD)[9–13] and elastic He scattering.[14,15] For explaining the x-ray diffraction results on the $p(2 \times 1)$ reconstruction, a model was proposed, based on a buckled array of disordered dimers with a 0.5 probability of finding one of the two dimer orientations

(positive and negative tilt angles) in any unit cell.[13] Additional complications in determining the dynamic structure may occur due to in-row as well as row-to-row disorder, which results in the appearance of various reconstruction domains. Due to the weak row-to-row interaction, the long-range ordering is strongly temperature dependent and the rows may be disordered for the observed $p(2 \times 1)$ reconstruction at 300 K.[14] The difference in the short- (between dimers) and long-range (between rows) interactions within the surface reconstruction leads to an asymmetric surface stress distribution which is compressive along the substrate dimer row direction and tensile stress in a direction perpendicular to the substrate dimer rows.[16] The coexistence of $p(2 \times 1)$ and $c(4 \times 2)$ was identified as one of the essential mechanisms for the relaxation of the surface stress.[5]

At lower temperatures (i.e., reduced thermal energy) the dimer rows form a well-ordered $c(4 \times 2)$ reconstruction. This reconstruction was identified as a ground state with lowest energy of the above-mentioned possible reconstruction and is clearly identified by all mentioned structural investigation methods including XRD.[17] The antiferromagnetic order of the dimer orientations reduces greatly the dipole interaction energy.[1] The temperature range which is reported for the transition between the ordered $c(4 \times 2)$ and the disordered $p(2 \times 1)/c(4 \times 2)$ is between 100 and 250 K .[14,17,18] STM images at 300 K by Zandvliet *et al.* show all three surface reconstructions coexisting on samples with a defect concentration above 0.2%, while for lower defect concentrations only the $p(2 \times 1)$ and $c(4 \times 2)$ reconstruction occur.[1,4,5] This difference might be due to a defect-induced local inhibition of dimer flipping. The experimental results reveal a double-domain structure, consisting of two types of regions, separated by monatomic steps. Each step induces a rotation of the dimer-row orientation by 90°. For vicinal surfaces, the coexistence of both domains was evidenced for miscut angles towards [110] as high as 5.4°.[7]
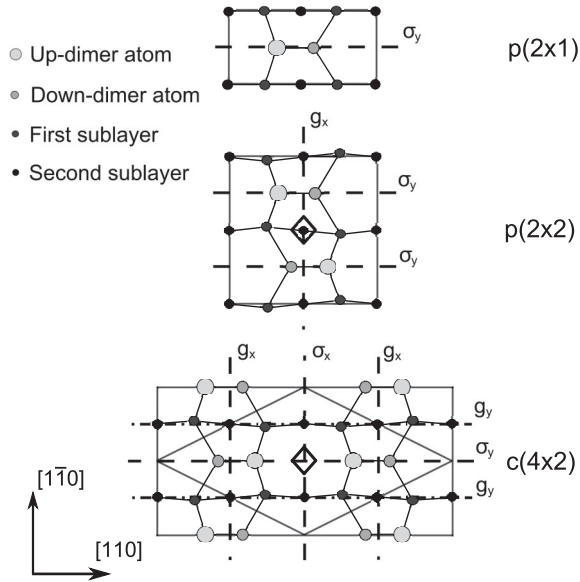
FIG. 1. Top view of the $p(2 \times 1)$, $p(2 \times 2)$, and $c(4 \times 2)$ Ge(001) surface reconstructions. The large-size circles represent the buckle-up dimer atoms, the middle-size circles the buckle-down ones, while the small circles belong to the atoms of the first and second sublayer (gray and black circles, respectively). The unit cells are indicated by a rectangle, a square, and a diamond, respectively. The dashed and dash-dotted lines indicate the mirror symmetry elements.

Since for the reconstructed surface the number of Ge atoms in the surface unit cell is much higher than for the bulk, a large number of surface vibration eigenmodes is expected. Moreover, these modes should be affected by the different reconstruction states and by the degree of disorder. An especially intriguing question concerns the possible impact of the dimer flipping in the $p(2 \times 1)$ reconstruction. The surface phonons of Ge(001) have been addressed with density-functional perturbation theory and local-coupling transfer[8,19] and within the adiabatic bond charge model.[20] Experimentally, the Rayleigh wave and optical surface modes in the energy range up to 7 meV have been reported from inelastic He atom scattering at room temperature for the $p(2 \times 1)/c(4 \times 2)$ phase.[8]

In this paper we report on the observation of surface vibration modes by Raman spectroscopy on Ge(001) at 300 and 40 K, that is, for the $p(2 \times 1)/c(4 \times 2)$ with flipping dimers and the static $c(4 \times 2)$ reconstruction, respectively. For the interpretation of the observed eigenmodes the Raman selection rules are exploited, giving access to the symmetry of the displacement patterns of the eigenmodes.

The paper starts with a description of surface Raman spectroscopy with special emphasis on symmetry considerations, which are reflected in the Raman tensors. After a survey of the sample preparation procedure and the experimental setup, the results are presented and compared with calculations by Tütüncü *et al.*[20] and Stigler *et al.*[8,19] Symmetry consequences of the dimer flipping and the row-to-row correlation will turn out as key arguments for the consistent mode assignment.

II. EXPERIMENT

The preparation procedure of the commercially available n-doped Ge(001) samples with a miscut angle below $0.5°$

consists of an *ex situ* wet-chemical etching process and *in situ* flash annealing with direct current heating, as described in Ref. 21. In detail, first the *ex situ* process started with ultrasonic cleaning, stirring, etching in a Piranha solution, and rinsing. Subsequently, for passivation, a thermal oxide layer was grown at 380 °C for 5 min (this temperature provides the activation energy for the oxidation[22]). Thereafter, the samples were transferred into the UHV optical chamber with a base pressure $\leqslant 2 \times 10^{-10}$ mbar. Degassing of the sample was performed for 8 h at 250 °C. Finally, the Ge surface was deoxidized *in situ* by flash annealing at 700 °C by direct current heating. The *ex situ* grown oxide desorbs, following the equation[23]

$$GeO_2 + Ge \rightarrow 2GeO \quad (T = 400 °C) \tag{1}$$

and a complete conversion of Ge-dioxide into the gaseous Ge-monoxide phase results.[21] The flash time was chosen as low as 1 s to minimize contamination due to the possible reaction between the hot surface and the residual gas in the UHV chamber.

In order to verify the surface quality and its reconstruction we employed LEED. For the study of the vibration modes by *in situ* Raman spectroscopy, we used a triple Dilor XY spectrograph with a silicon based CCD detector, and a solid state laser (532 nm) as excitation source. The excitation energy is closely matched to the electronic E_1 transition of bulk Ge in order to ensure resonant Raman excitation conditions and a minimum penetration depth of light. For temperature-dependent studies of the vibration modes and the impact of reconstruction phase transitions, cooling can be achieved by a closed cycle helium cryostat, enabling Raman spectroscopy at low temperatures.

III. SURFACE RAMAN SPECTROSCOPY

The displacement pattern of surface vibration modes is confined to a few topmost atomic layers, according to the surface confinement of the individual mode. Therefore, the scattering intensity of surface phonons is expected to be far below the bulk phonon intensity, due to the extremely small scattering volume.[24] However, when exploiting resonances at electronic transition energies a sufficient sensitivity for detecting and analyzing surface phonons by Raman spectroscopy is achieved.[25,26]

Raman scattering with a defined light polarization configuration gives not only access to the vibration mode energies, but also reveals their symmetry by exploiting symmetry-induced selection rules, which are derived from the Raman tensors for the crystallographic point groups. These tensors are discussed in the following for deformation potential (DP) scattering.[27]

The surface reconstruction $p(2 \times 1)$ has a rectangular unit cell and one mirror plane σ_y shown in Fig. 1 and belongs to the point group m and the plane group Pm (monoclinic). The DP Raman tensors for the point group m are[28]

$$A_1 = \begin{pmatrix} a & d & \\ e & \mathbf{b} & \\ & & \mathbf{c} \end{pmatrix} \quad \text{and} \quad A_2 = \begin{pmatrix} & & j \\ & & \mathbf{h} \\ g & \mathbf{i} & \end{pmatrix}. \tag{2}$$

Following the conventional notation of optical spectroscopy, the surface normal is denoted as x axis, and the

in-plane directions are denoted as y and z axes. Therefore, in backscattering geometry the relevant tensor elements are yy, zz, yz, and zy, due to the transversal character of the light waves. For (001) surface phonon modes, the nonvanishing relevant tensor elements, that is, **b** and **c** of the A_1 tensor and **i** and **h** of the A_2 tensor, reflect the possible mode symmetries and dictate the selection rules for each mode. The A_1 tensor implies Raman intensity proportional to b^2 or c^2 for parallel polarization directions of incident and scattered light along one of the principal axes of the surface coordinate system (i.e., the [110] or the [1$\bar{1}$0] direction of the cubic bulk cell), while the A_2 induces intensity proportional to h^2 or i^2 for perpendicular polarizations along these axes.

The $p(2 \times 2)$ surface reconstruction belongs to the point group $2mm$ and the plane group $P2mg$ (orthorhombic), due to the rectangular unit cell with a twofold rotation axis, a glide plane g_x, and two mirror planes σ_y, as illustrated in Fig. 1. The corresponding DP Raman tensors according to Ref. 28 are

$$
A_1 = \begin{pmatrix} a & & \\ & \mathbf{b} & \\ & & \mathbf{c} \end{pmatrix}, \quad A_2 = \begin{pmatrix} & & d \\ e & & \\ & & \end{pmatrix},
$$

$$
B_1 = \begin{pmatrix} & & f \\ & & \\ g & & \end{pmatrix}, \quad \text{and} \quad B_2 = \begin{pmatrix} & & \\ & & \mathbf{h} \\ & \mathbf{i} & \end{pmatrix}. \tag{3}
$$

The $c(4 \times 2)$ surface reconstruction contains a diamond-shape unit cell with a twofold rotation axis, two mirror planes σ_x and σ_y, two glide planes g_x, and two glide planes g_y. It belongs to the plane group $c2mm$ and the point group $2mm$. The Raman tensors and the corresponding selection rules are identical with the $p(2 \times 2)$ reconstruction.[28]

IV. RESULTS AND DISCUSSION

A. LEED characterization

Figure 2 shows the LEED pattern, taken at 300 K with an electron energy of 34 eV from a Ge(001) surface, prepared along the above-described procedure. The spots correspond to a two-domain $p(2 \times 1)$reconstruction structure. Note, however, also the streaks which appear between the spots of the $p(2 \times 1)$. They show an enhanced intensity at sites which correspond to the $c(4 \times 2)$ reconstruction. In literature they are assigned to thermally activated frequent flip-flop motions
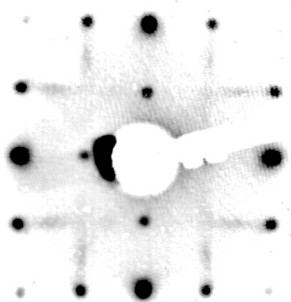
FIG. 2. LEED pattern at 34 eV of a Ge(001) surface with a $p(2 \times 1)/c(4 \times 2)$ reconstruction, indicated by streaks between the spots.

of the buckled dimers.[6] Thus, the surface has a two-domain $p(2 \times 1)/c(4 \times 2)$ reconstruction, as it is common for Ge(001) at 300 K.[1]

B. Polarized Raman spectroscopy at 300 K

Raman spectra were recorded *in situ* in UHV at 300 and 40 K before and after the flash annealing preparation, that is, on the Ge(001) surface with thermal oxide and on the reconstructed $p(2 \times 1)/c(4 \times 2)$ Ge(001) surface. In this way we obtain the vibrational characteristics of the penultimate and the final preparation stage of the surface and subsequently separate the features which are induced by the surface reconstruction. The 300 K results are shown in Fig. 3. Figure 3(a) represents the spectra for parallel polarization of the incident and scattered light along one of the in-plane principal axes.
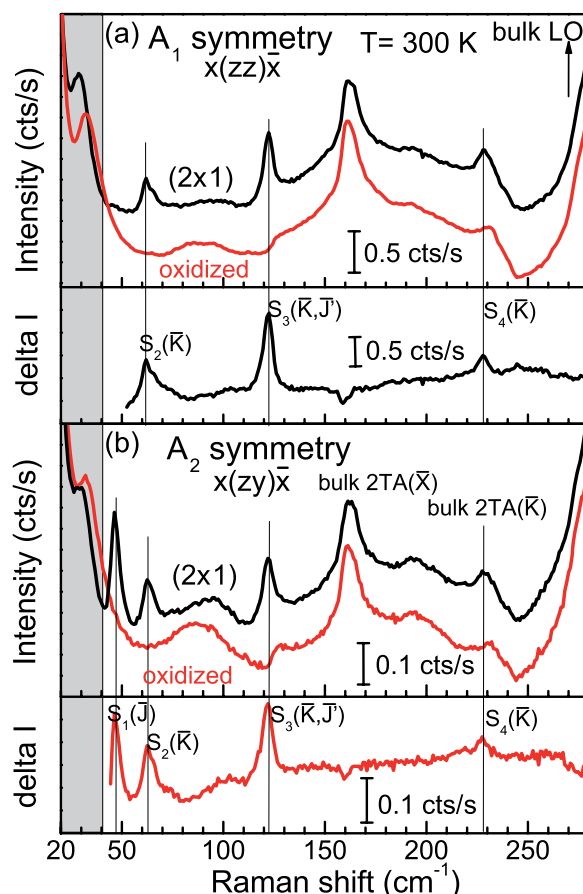
FIG. 3. (Color online) Raman spectra of Ge(001) at 300 K for (a) A_1 symmetry and (b) for A_2. The red spectra originate from thermally oxidized Ge, the black ones from the two-domain $p(2 \times 1)/c(4 \times 2)$ reconstruction after flash-cleaning. Below each pair of spectra their intensity difference ΔI is plotted. The gray background marks the range below 40 cm^{-1}, which is inaccessible for surface phonon studies because of a substrate peak and the edge of the laser line. Oxidized Ge only shows two acoustic bulk phonon modes [2TA(X), 2TA(K)]. The clean reconstructed Ge(001) surface shows three additional phonon modes for the parallel polarization configuration (a) $x(zz)\bar{x}$, and four modes for the configuration (b) $x(zy)\bar{x}$. Their nomenclature indicates their assignment to the eigenmodes, calculated in Ref. 20.

Following the optical convention, the surface normal is named the x axis. The in-plane axis of light polarization is denoted here as the z axis. This scattering configuration is denoted as $x(zz)\overline{x}$ according to the established Porto notation.[28] The configuration with perpendicular polarization of the incident and the scattered light is shown in Fig. 3(b), and denoted as $x(zy)\overline{x}$.

The oxidized Ge sample shows the expected second-order vibrational Raman signature due to two-phonon scattering from bulk modes: At 163 cm^{-1} a clear peak from 2TA at the X point of the Brillouin zone (BZ) and at 228 cm^{-1} an edge-like structure from 2TA at the K point.[29,30] The rising intensity toward the high-energy edge of the spectrum originates from first-order Raman scattering of the bulk optical phonon, whose peak is located at 302 cm^{-1} and exceeds the 2TA intensity by a factor of 20. Furthermore, near the low-energy edge a peak at 30 cm^{-1} appears, which originates from electronic Raman scattering[31,32] due to the substrate doping. This peak and the increasing intensity toward the low-energy edge of the spectrum due to the laser line hamper the detection of possible surface phonons below 40 cm^{-1}. Therefore this region is marked by the gray background.

Figure 3 also shows the 300 K Raman spectra of the flash-cleaned $p(2 \times 1)/c(4 \times 2)$ reconstructed Ge(001) surface for the polarization configurations $x(zz)\overline{x}$ [Fig. 3(a)] and $x(zy)\overline{x}$ [Fig. 3(b)]. Due to the two-domain surface, in the polarization configuration $x(zz)\overline{x}$, that is, with parallel polarizations along z, not only Raman scattering by the tensor element zz is observed, but also from the orthogonally oriented complementary domains by the element yy. Macroscopically no distinction can be made between along-row polarization and perpendicular-to-row polarization. In the spectra from the reconstructed surface, besides the second-order features from the bulk Ge, additional new peaks appear at 46, 62, 122, and 227 cm^{-1} (i.e., 5.70, 7.69, 15.13, and 28.15 meV). For a clearer distinction of these new peaks, Fig. 3 additionally shows below each panel the intensity difference ΔI of the spectra from the flash-cleaned and the oxidized surface. For the off-diagonal configuration (b) the four peaks all appear, while for the diagonal case (a) the low-frequency peak (46 cm^{-1}) is missing. Additionally, we would like to note that also the deposition of Au on the Ge surface, inducing a $c(8 \times 2)$ reconstruction, induces the complete disappearance of the features S_1 to S_4. The newly observed Raman peaks are attributed to reconstruction-induced surface vibration modes, and are denoted as S_1 to S_4 with indices $\overline{J}$, $\overline{J}'$, $\overline{K}$. These indices will be explained below when assigning mode patterns and q vectors.

The observed surface peak frequencies correspond very well to the results from Tütüncü *et al.*[20] and Stigler *et al.*,[8,19] calculated for the Ge(001) (2×1) reconstruction by means of the adiabatic bond-charge model and density-functional perturbation theory, respectively. The surface phonon dispersion Fig. 4 and eigenmode displacements Fig. 5 given in Ref. 20 are particularly useful for the following discussion of our Raman spectra.

C. Surface vibration mode identification

The identification of the observed surface phonons in terms of characteristic mode patterns is performed by means of the calculated dispersion curves of Ref. 20. Figure 4 shows as
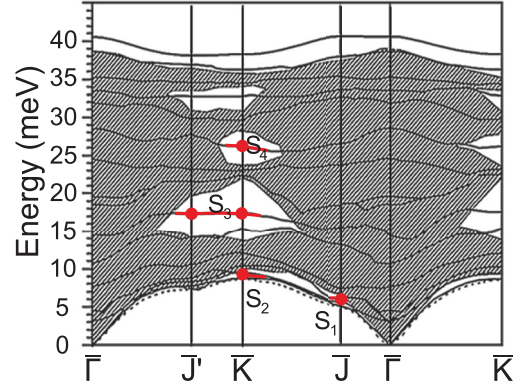
FIG. 4. (Color online) Full lines: Surfaces phonon dispersion curves of Ge(001) $p(2 \times 1)$, calculated within the adiabatic bond charge model. The dashed area is the projected bulk phonon dispersion range (from Ref. 20). The observed Raman peaks belong to the curves S_1 to S_4 in the range of the q vectors which are marked by circles.

full lines these surface phonon dispersion branches along the high-symmetry directions of the $p(2 \times 1)$ surface BZ: Wave vectors on the $\overline{\Gamma}$ to $\overline{J}'$ line point along the dimer rows, that is, in direction [1$\overline{1}$0], while $\overline{\Gamma}$ to $\overline{J}$ represents the row-to-row direction [110]. The flat dispersion reflects the weakness of the dimer-to-dimer interaction within each row and the even weaker row-to-row interaction with respect to the vibrational energy within the dimer-based unit.

Confinement to the surface is only expected for those modes whose frequency ω and surface wave vector $\mathbf{q}_{||}$ do not match the $(\omega, \mathbf{q}_{||})$ pair of a bulk phonon mode. The ensemble of the bulk $(\omega, \mathbf{q}_{||})$ pairs is shown in Fig. 4 as a dashed area, which covers the large majority of the calculated surface phonon branches and leaves only a few gaps. No gap occurs at $\overline{\Gamma}$
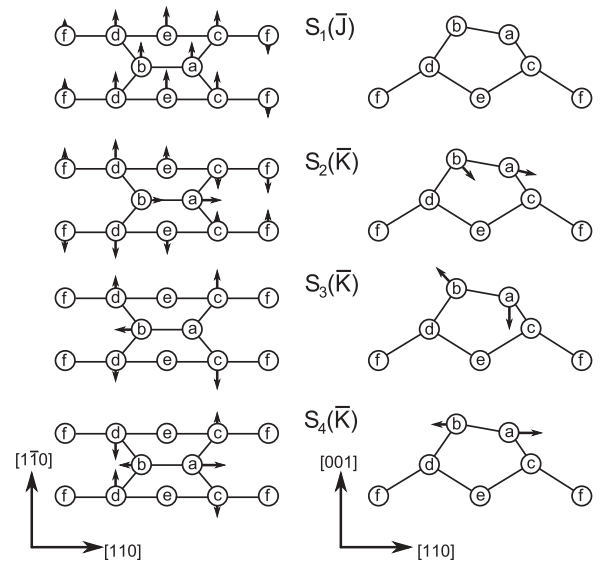
FIG. 5. Top view (left side) and side view (right side) of the displacement patterns, calculated in Ref. 20, for the surface phonon modes which are observed as Raman peaks. The $S_4(\overline{K})$ dimer stretch and backbond twist mode, the $S_3(\overline{K})$ dimer rocking mode, and the $S_2(\overline{K})$ are optical modes. The $S_1(\overline{J})$ is a transverse acoustic mode.

because in the diamondlike Ge lattice the bulk longitudinal acoustic (LA) phonon branch in the [001] direction touches the longitudinal optical (LO) phonon branch at the BZ edge X, which is projected onto the surface BZ center $\overline{\Gamma}$. Therefore, for the $p(2 \times 1)$ reconstructed surface all surface phonons with vanishing transversal wave vector are expected to decay into bulk modes. This results in a significantly reduced surface-phonon lifetime, that is, a strong damping, which will hamper or even impede its observation in the Raman spectrum.

For the three Raman peaks at 62, 122, and 227 cm^{-1}, a further argument against their assignment to modes at $\overline{\Gamma}$ is their occurrence for both polarization configurations. While the calculated displacement patterns of the $\overline{\Gamma}$-point vibrations have a symmetry-conserving character, for which the A_1 Raman tensor applies, the experimentally observed phonons obviously contain components from both A_1 and A_2 symmetry.

When considering the bulk-gap criterion in the phonon dispersion diagram together with the characteristic frequency range of each phonon branch, only four surface phonon branches remain for the assignment of the observed peaks. They are marked in Fig. 4 as S_1 to S_4. We attribute the 46 cm^{-1} peak to the $\overline{J}$ point of the lowest calculated dispersion branch S_1 and denote it as $S_1(\overline{J})$. The 62 cm^{-1} peak is assigned to the $\overline{K}$ point of the S_2 branch, and named $S_2(\overline{K})$. The 122 cm^{-1} peak fits to the S_3 branch at $\overline{K}$ as well as at $\overline{J}'$ and the range in between. It is termed $S_3(\overline{K}, \overline{J}')$. Finally, the 227 cm^{-1} peak is assigned to the $\overline{K}$ range of the S_4 phonon branch, and named $S_4(\overline{K})$. The difference between the experimentally observed surface mode frequencies and the calculations is in the range of 1 to 2 meV. This is comparable to the difference between experiment and calculation for the bulk mode at the BZ center, calculated in Ref. 20 as 38.6 meV (311 cm^{-1}), and experimentally observed at 37.2 meV (300 cm^{-1}).

D. Surface phonon displacement patterns

In Fig. 4 the relevant high-symmetry points and adjacent q regions of the dispersion curves S_1 to S_4 are marked by circles and bold lines, respectively. The corresponding mode patterns at $\overline{K}$ and $\overline{J}$ according to Ref. 20 are shown in Fig. 5. The pattern of the $S_4(\overline{K})$ mode consists of a dimer stretch and backbond twist, while the $S_3(\overline{K})$ mode is a dimer rocking. The $S_2(\overline{K})$ mode corresponds to a vibration of the first-layer atoms with components in both the surface normal and dimer bond directions, while the second-layer atoms move in the dimer row direction. In contrast to the optical character of these three modes, $S_1(\overline{J})$ is a transverse acoustic mode. Its nonzero frequency is purely due to its finite wave vector in row-to-row direction. The symmetry of the mode patterns is in accordance with the polarization dependence of their Raman peaks: $S_1(\overline{J})$ is purely asymmetric with respect to the mirror plane perpendicular to the dimer rows. It is referred to as a shear horizontal (SH) polarization mode.[19] This symmetry type gives rise only to off-diagonal scattering. In the modes $S_2(\overline{K})$ to S$_4(\overline{K})$ an SH polarization component is superimposed with a sagittal plane (SP) polarization component, that is, a polarization component in the plane of the wave vector and surface normal. This component is symmetric with respect to the mirror plane and gives rise to diagonal scattering. Therefore, these three modes appear in both polarization configurations.

E. Phonon wave vector consideration

The first-order Raman scattering from surface modes at the BZ edge points $\overline{J}$, $\overline{J}'$, and $\overline{K}$, that is, from modes with very large $\mathbf{q}_{||}$ vectors, is highly intriguing. It seems to contradict the fundamental law of q-vector conservation. The solution of this remarkable finding will turn out as a key result of this study.

For explaining this difference we consider the dynamic character of the $p(2 \times 1)$ reconstruction, that is, the flip-flop motion of the buckled dimers.[1] STM results are explained within a model that describes a collective dynamic buckling of the surface dimers and takes into account strain relaxation energy and domain wall formation energy.[5] Based on entropy arguments, it is estimated that in a dimer row on average about 30 antiferromagnetically (AF) ordered buckled dimers flip collectively, which implies a conservation of the in-row AF buckling order on a short-length scale. This short-scale order conservation seems reasonable because the AF configuration of in-row neighbor dimers is energetically favorable by 86.7 meV/dimer according to density-functional calculations.[33] Within such an AF-configured region, the in-row periodicity consists of two dimers, which corresponds to the zone-edge point $\overline{J}'$ of the $p(2 \times 1)$ reconstruction in reciprocal space (see Fig. 6).

For assessing the required spatial correlation length for observing Raman scattering along this scenario, we must be aware that optical phonon modes primarily probe short-scale order because of the dominance of nearest- and next-nearest neighbor interaction forces in lattice dynamics. As an example, a systematic Raman study on nanocrystalline Si has revealed that already for a correlation length as low as 3.5 nm its phonon peak width is as narrow as for a single crystal.[34] Therefore, the impact of a reduced coherence and finite-size effects is in Raman scattering substantially lower than in diffraction experiments such as LEED and x-ray diffraction. This might also be a possible reason for the experimental finding that x-ray data of the $p(2 \times 1)$ are best described within a model of disordered dimer buckling.[13] Furthermore, the two alternating AF dimer buckling configurations are equivalent for the surface vibrations. Therefore, the STM-typical time averaging of complementary signatures of both buckling states, which results in the appearingly symmetric
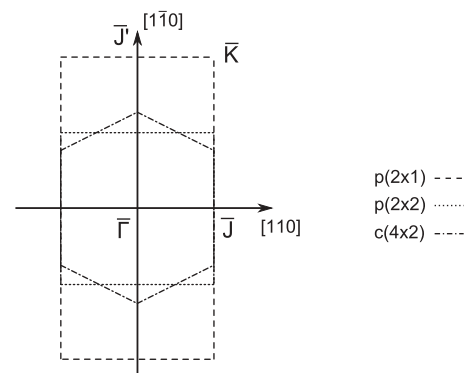
FIG. 6. Surface Brillouin zones for the three possible surface reconstructions $p(2 \times 1)$, $p(2 \times 2)$, and $c(4 \times 2)$. In the $p(2 \times 2)$ reconstruction, the $\overline{J}'$ point of the $p(2 \times 1)$ is backfolded to $\overline{\Gamma}$. In the $c(4 \times 2)$ reconstruction, the $\overline{K}$ point of the $p(2 \times 1)$ is backfolded to $\overline{\Gamma}$.

dimers, does not occur in light scattering. The time-integrated (continuous wave, cw) Raman result may be considered as an integrated series of equivalent snapshot spectra on the phonon time scale. For comparing the phonon time scale with the dimer flipping frequency, data from time-resolved STM experiments are available.[35,36] These data reveal that the flip-flop motion of the dimers takes place on a time scale in the range of a millisecond to some 10 μs, that is, way slower than the phonon oscillation period (on the order of a picosecond) and lifetime (<nanosecond). Thus, the surface vibrations experience a quasistatic configuration of small groups of AF-buckled dimers.

In fact, the AF ordering of buckled dimers is compatible to a $p(2 \times 2)$ reconstruction. When examining the LEED pattern for independent experimental evidence of this $p(2 \times 2)$ phase, it is noted that in the angular region which corresponds to (2×2) diffraction peaks, the LEED image only shows stripes and some residual intensity. Quite similar observations were reported in literature for Si(001) above the transition temperature from $c(4 \times 2)$ to $p(2 \times 1)$.[37] The weakness and streaky nature of the (2×2)-related signature in our LEED image strongly indicate that the domain size is insufficient for generating well-defined (2×2) diffraction peaks, although it does allow the much more localized Raman process from phonons of this reconstruction. The possibility of thermally activated collective fluctuations of such small patches, consisting of groups of about 30 dimers, as reported in literature,[5] is fully compatible with our Raman observations. Due to the very fast time scale of the phonon vibrations, their occurrence is compatible with a comparatively slower flipping of groups of AF buckled dimers as well as with static $p(2 \times 2)$ patches. However, STM reports indicate that such static patches very rarely occur on high-quality surfaces.[1,4,5] In principle, quasistatic nonflipping $p(2 \times 2)$ regions which are pinned at defects cannot be strictly excluded as the origin of our Raman signals, but this source seems rather improbable, because the Raman scattering intensity of such sporadic patches is expected to be below our detection limit. Generally, the literature reports of Raman results from semiconductor surface vibration modes pertain to fully or at least substantially covered surfaces.[24]

F. Correlation with the $p(2 \times 1)/c(4 \times 2)$ reconstruction

This perception puts forward the question of the enduring relevance of the $p(2 \times 1)$-based calculated dispersion curves. Regarding the vibration frequencies, only minor effects are expected when locally doubling the in-row periodicity of the $p(2 \times 1)$ since the vibration dynamics is essentially determined within the dimer unit cell, and coupling to adjacent dimers is comparatively weak. The direct calculation of surface phonons for the higher-order reconstructions is hampered by the large number of atoms in their unit cells. This problem is circumvented by Stigler *et al.* in a symmetry-based approach, denoted as local-coupling transfer (LCT).[8,19] For a doubled in-row periodicity they obtain a prominent mode at 7 eV, rocking modes in the range of 12.7 to 15.2 meV, and also the stretch-and-twist mode at 28 meV. These frequency values also apply for the $c(4 \times 2)$.

For a check of the impact of the enhanced in-row periodicity on the wave vectors, Fig. 6 shows the first Brillouin zone of

the reconstructions $p(2 \times 1)$, $p(2 \times 2)$, and $c(4 \times 2)$. As seen from this plot, the $\overline{J}'$ point of the $p(2 \times 1)$ Brillouin zone is backfolded to $\overline{\Gamma}$ in the $p(2 \times 2)$, and Raman scattering from $S_3(\overline{J}')$ is allowed. Due to the displacement pattern, it may occur in A_1 as well as A_2 symmetry.

Moreover, the dimer flipping, which according to Ref. 5 occurs collectively for groups of about 30 dimers in a row, disturbs the row-to-row coherence of the dimer buckling. Hereby, the conservation of the q-vector component perpendicular to the rows is relaxed, that is, in the direction from $\overline{J}'$ to $\overline{K}$ and from $\overline{\Gamma}$ to $\overline{J}$. As a consequence, the ranges around the $\overline{K}$ point and the $\overline{J}$ point of the $p(2 \times 1)$ surface Brillouin zone become accessible. The $\overline{K}$ range justifies the scattering intensity from $S_2(\overline{K})$, $S_3(\overline{K})$, $S_4(\overline{K})$, whose mode patterns also comprise both symmetry components A_1 and A_2. Due to the flatness of the surface phonon dispersion branches, the scattering contributions from the various q ranges induce virtually no peak broadening, but instead result in a significant peak intensity enhancement.

The absence of the upper calculated surface phonon branch (range 38 to 40 meV) in the experimental spectra is most probably due to its close proximity to the bulk phonon, whose scattering intensity is much stronger. In the range of $\overline{J}'$ and $\overline{K}$ its frequency even fully coincides with the bulk phonon at Γ. Besides, the intensity of each symmetry-allowed mode in the Raman spectrum is governed by its electron-phonon coupling strength, also referred to as its Raman activity.[28] This may vary strongly from mode to mode, because the overall electron-phonon coupling strength reflects the net change of the electronic dielectric susceptibility by the vibration-induced lattice deformation. Depending on the mode pattern, the contributions of the involved electronic bonds may enhance each other, but may also be mutually compensating. Thus, the strength of the deformation potential may vary strongly, as shown, for example, for vibration modes of Sb on GaAs(110).[27] This might be a possible reason for the absence of the calculated mode at about 33 meV in the experimental spectra. Furthermore, it has to be considered that by the q vector backfolding in the reconstructions beyond $p(2 \times 1)$ the relevance of surface-mode damping due to overlap with projected bulk modes distinctly increases. The quantitative impact is expected to be mode dependent since it is determined by the surface mode pattern as well as by the bulk density-of-states at the relevant frequency.

G. Polarized Raman spectroscopy at 40 K

Figure 7 shows the Raman scattering spectra at 40 K of the thermally oxidized and the reconstructed Ge(001) surface, in both polarization configurations $x(zz)\overline{x}$ and $x(zy)\overline{x}$. As expected, the second-order scattering from the vibrational bulk phonon modes $2TA(X)$ (163 cm^{-1}) and $2TA(K)$ (228 cm^{-1}), which were prominently observed at 300 K, have nearly vanished now as a result of the reduced Bose-Einstein factor $n(\omega,T)$. The T dependence of the intensity for second-order scattering is much more pronounced than for first order, because the first-order intensity at frequency ω is proportional to $[n(\omega,T) + 1]$, while for the second-order scattering at this frequency the square of $[n(\omega/2,T) + 1]$ applies.[28,38] For the second-order scattering at 163 cm^{-1} the temperature reduction
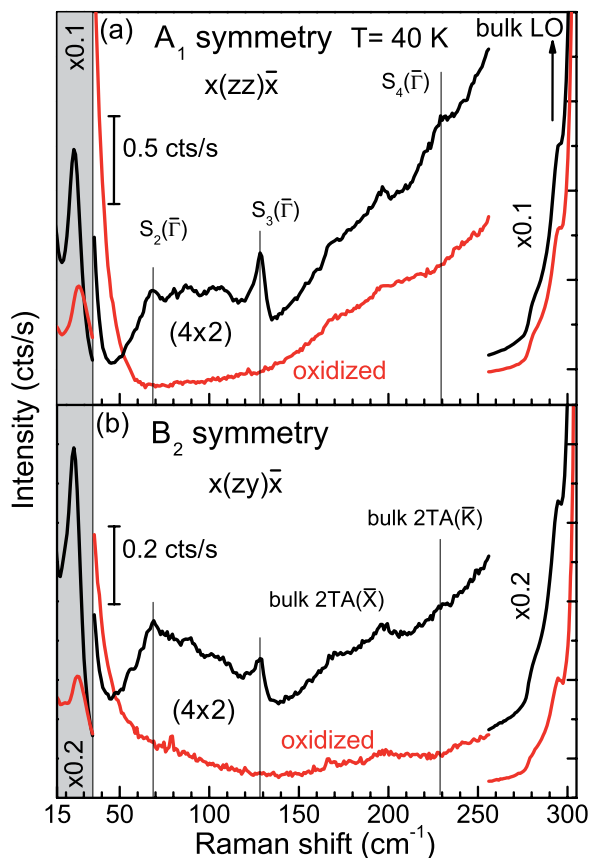
FIG. 7. (Color online) Raman spectra of Ge(001) at 40 K for (a) A_1 symmetry [polarization configuration $x(zz)\overline{x}$] and for (b) A_2 [configuration $x(zy)\overline{x}$]. The red spectra originate from thermally oxidized Ge, the black ones from the $c(4 \times 2)$ reconstruction after flash-cleaning. The second-order bulk features have nearly vanished. The optical surface phonon peaks from the dispersion branches S_2 to S_4 persist, while the acoustic mode $S_1(\overline{J})$ has vanished.

from 300 to 40 K implies a decrease by 88%. At the low-energy edge of the Raman spectrum, the electronic excitation mode persists. As for the surface phonon modes, the comparison with the 300 K spectra shows that the peaks from the S_2, S_3, and S_4 branches persist. They occur at 68, 127, and 227 cm^{-1}, respectively. In contrast, the acoustic mode $S_1(\overline{J})$ has vanished.

H. Correlation with the $c(4 \times 2)$ reconstruction

At 40 K the Ge(001) surface has an ordered static $c(4 \times 2)$ reconstruction.[14,17,18] As illustrated in Fig. 1, this is a higher-order structure, based on the $p(2 \times 1)$ unit mesh. Therefore, also for this symmetry the expected phonon behavior may be derived from the $p(2 \times 1)$ calculation results, which are presented in Fig. 4. The vibration mode frequencies are expected to be essentially invariant since the dimer-to-dimer and row-to-row interaction energies are significantly smaller than those within the $p(2 \times 1)$ unit cell. This expectation is confirmed by the results of the local-coupling transfer (LCT) calculations by Stigler *et al.*[19]

For the determination of the q-vector regions that may contribute to the Raman scattering process, the larger size of the low-temperature $c(4 \times 2)$ unit cell and also the substantially

enhanced ordering in the row-to-row direction due to the disappearance of the $p(2 \times 1)$ domains must be considered. The size and symmetry of the enlarged $c(4 \times 2)$ unit cell determine the criteria for finite q vectors of the $p(2 \times 1)$ to end up in the BZ center $\overline{\Gamma}$ of the $c(4 \times 2)$. The ordering implies that the scattering is essentially confined to the BZ center $\overline{\Gamma}$, in contrast to the case of the patterned domains at 300 K. The q-vector selection is illustrated in Fig. 6, showing the first BZ of $p(2 \times 1)$, $p(2 \times 2)$, and $c(4 \times 2)$. The distance from $\overline{\Gamma}$ to the $\overline{K}$ point of the $p(2 \times 1)$ is exactly twice the extent of the first BZ of $c(4 \times 2)$ in this direction. Therefore, the $\overline{K}$ point of $p(2 \times 1)$ corresponds to the BZ center of $c(4 \times 2)$. The $p(2 \times 1)$ $\overline{J}$ point remains at the BZ edge also for $c(4 \times 2)$. Considering the direction towards $\overline{J}'$, the extent of the $c(4 \times 2)$ BZ is 62.5% of the $p(2 \times 1)$. Therefore, the zone-edge point $\overline{J}'$ of $p(2 \times 1)$ does not correspond to any high-symmetry position in $c(4 \times 2)$. Thus, only $\overline{K}$ of $p(2 \times 1)$ represents the full symmetry of $c(4 \times 2)$. The same result is obtained by considering that in the $c(4 \times 2)$ a sign reversal of the dimer tilt occurs in the in-row as well as in the row-to-row direction. As illustrated in Fig. 5, this sign-reversal symmetry along both directions is only fulfilled by modes at the $\overline{K}$ point of the $p(2 \times 1)$ BZ.

Because of these symmetry considerations, the peaks from the surface phonon branches S_2, S_3, and S_4 in Fig. 7, which were attributed at 300 K to the $\overline{K}$ region of the BZ, are denoted now as $\overline{\Gamma}$ peaks. These considerations also explain why the $S_1(\overline{J})$ peak, whose $p(2 \times 1)$ q vector does not correspond to the $c(4 \times 2)$ BZ center, is missing in the 40 K spectra. The experimental results underscore the much stricter requirement for q-vector conservation in the light scattering process due to the strongly improved long-range ordering of the $c(4 \times 2)$ surface structure. The mode frequencies of $S_2(\overline{\Gamma})$, $S_3(\overline{\Gamma})$, and $S_4(\overline{\Gamma})$, which amount to 68, 127, and 227 cm^{-1}, respectively, are very close to those at 300 K. These data confirm the results of the LCT model calculations, which yield a very close vibration frequency correspondence between $p(2 \times 2)$ and $c(4 \times 2)$.[19] These calculations also show that the relatively low-peak intensity might be attributed to damping due to decay into bulk modes. As discussed already for the 300 K results, the occurrence of the surface phonon modes in both polarization configurations is a consequence of the atomic displacement symmetry within the dimer unit cell.

In the energy range from 68 to 127 cm^{-1} a quasicontinuum is observed, which cannot be assigned either to a specific surface reconstruction or a specific symmetry. In the theoretical and experimental work from Stigler *et al.* a rocking mode occurs at 300 K for the $p(2 \times 2)$ and $c(4 \times 2)$ reconstruction that produces weak peaks in the inelastic helium scattering intensity in the energy range from 104 to 116 cm^{-1}.[8] On the other hand, none of the existing theory results predicts phonon frequencies which cover the total interval of the observed quasicontinuum signal. Therefore, further investigation seems required for explaining this feature.

V. SUMMARY

In polarized Raman spectroscopy experiments on flash-cleaned reconstructed Ge(001) we have observed four surface phonon modes for the $p(2 \times 1)/c(4 \times 2)$ reconstruction at 300 K. Their energy eigenvalues are 5.70, 7.69, 15.13,

and 28.15 meV. They are in good agreement with results from the adiabatic bond charge model and from density-functional perturbation theory. The surface phonon modes seemingly originate from the BZ edge region of the $p(2 \times 1)$ reconstruction. However, a closer inspection of the relevant time scales reveals that the surface phonon oscillations are insensitive for the comparatively slow periodic dimer flipping, which induces the $p(2 \times 1)$ as a time average. Because of the short-range instantaneous antiferromagnetic in-row order of flipping buckled dimers, the relevant wave vector is the zone-edge $\overline{J}'$ of the $p(2 \times 1)$ BZ. For the static $c(4 \times 2)$ reconstruction at 40 K, the q-vector conservation is fulfilled far more strictly. In the Raman spectra, only those modes remain whose wave vector is backfolded to the $c(4 \times 2)$ BZ center.

Therefore, the mode at 5.70 meV vanishes. A quintessence of our experiments is that in Raman scattering the impact of the periodic dimer flipping in the $p(2 \times 1)$ reconstruction is distinct to that in LEED, x-ray, and STM experiments.

*eugen.speiser@isas.de

[1] H. J. W. Zandvliet, Phys. Rep. **388**, 1 (2003).

[2] C. Blumenstein, J. Schäfer, S. Mietke, S. Meyer, A. Dollinger, M. Lochner, X. Y. Cui, L. Patthey, R. Matzdorf, and R. Claessen, Nat. Phys. **7**, 776 (2011).

[3] J. A. Kubby, J. E. Griffith, R. S. Becker, and J. S. Vickers, Phys. Rev. B **36**, 6079 (1987).

[4] H. J. W. Zandvliet, B. S. Swartzentruber, W. Wulfhekel, B. J. Hattink, and B. Poelsema, Phys. Rev. B **57**, 6803R (1998).

[5] H. J. W. Zandvliet, R. van Gastel, O. Gurlu, and B. Poelsema, Phys. Lett. A **326**, 457 (2004).

[6] T. Shirasawa, S. Mizuno, and H. Tochihara, Surf. Sci. **600**, 815 (2006).

[7] C. Tegenkamp, J. Wollschläger, H. Pfnür, F. J. Meyer zu Heringdorf, and M. Horn-von Hoegen, Phys. Rev. B **65**, 235316 (2002).

[8] W. Stigler, P. Pavone, U. Schröder, J. Fritsch, G. Brusdeylins, T. Wach, and J. P. Toennies, Phys. Rev. Lett. **79**, 1090 (1997).

[9] R. Rossmann, H. Meyerheim, V. Jahns, J. Wever, W. Moritz, D. Wolf, D. Dornisch, and H. Schulz, Surf. Sci. **279**, 199 (1992).

[10] J. Alvarez, V. H. Etgens, X. Torrelles, H. A. van der Vegt, P. Fajardo, and S. Ferrer, Phys. Rev. B **54**, 5581 (1996).

[11] K. Terakura, T. Yamasaki, and Y. Morikawa, Phase Transitions **53**, 143 (1995).

[12] C. A. Lucas, C. S. Dower, D. F. McMorrow, G. C. L. Wong, F. J. Lamelas, and P. H. Fuoss, Phys. Rev. B **47**, 10375 (1993).

[13] X. Torrelles, H. van der Vegt, V. Etgens, P. Fajardo, J. Alvarez, and S. Ferrer, Surf. Sci. **364**, 242 (1996).

[14] R. Culbertson, Y. Kuk, and L. Feldman, Surf. Sci. **167**, 127 (1986).

[15] W. R. Lambert, P. L. Trevor, M. J. Cardillo, A. Sakai, and D. R. Hamann, Phys. Rev. B **35**, 8055 (1987).

[16] M. T. Middel, H. J. W. Zandvliet, and B. Poelsema, Phys. Rev. Lett. **88**, 196105 (2002).

[17] S. Ferrer, X. Torrelles, V. H. Etgens, H. A. van der Vegt, and P. Fajardo, Phys. Rev. Lett. **75**, 1771 (1995).

[18] S. D. Kevan, Phys. Rev. B **32**, 2344 (1985).

[19] W. Stigler, P. Pavone, and J. Fritsch, Phys. Rev. B **58**, 13686 (1998).

[20] H. M. Tütüncü, S. J. Jenkins, and G. P. Srivastava, Phys. Rev. B **57**, 4649 (1998).

[21] C. Blumenstein, S. Meyer, A. Ruff, B. Schmid, J. Schäer, and R. Claessen, J. Chem. Phys. **135**, 064201 (2011).

[22] A. Delabie, F. Bellenger, M. Houssa, T. Conard, S. V. Elshocht, M. Caymax, M. Heyns, and M. Meuris, Appl. Phys. Lett. **91**, 082904 (2007).

[23] Yoshiki and Kamata, Mater. Today **11**, 30 (2008).

[24] N. Esser, Appl. Phys. A **69**, 507 (1999).

[25] W. Richter, N. Esser, A. Kelnberger, and M. Köpp, Solid State Commun. **84**, 165 (1992).

[26] V. Wagner, J. Wagner, S. Gundel, L. Hansen, and J. Geurts, Phys. Rev. Lett. **89**, 166103 (2002).

[27] P. V. Santos, N. Esser, M. Cardona, W. G. Schmidt, and F. Bechstedt, Phys. Rev. B **52**, 12158 (1995).

[28] M. Cardona and G. Güntherodt, *Light Scattering in Solids II: Basic Concepts and Instrumentation*, edited by M. Cardona and G. Güntherodt (Springer, Berlin, 1982), Vol. 50 .

[29] B. A. Weinstein and M. Cardona, Phys. Rev. B **7**, 2545 (1973).

[30] S. Wei and M. Y. Chou, Phys. Rev. B **50**, 2221 (1994).

[31] J. Doehler, Phys. Rev. B **12**, 2917 (1975).

[32] C. H. Henry, J. J. Hopfield, and L. C. Luther, Phys. Rev. Lett. **17**, 1178 (1966).

[33] Y. Yoshimoto, Y. Nakamura, H. Kawai, M. Tsukada, and M. Nakayama, Phys. Rev. B **61**, 1965 (2000).

[34] H. Richter, Z. Wang, and L. Ley, Solid State Commun. **39**, 625 (1981).

[35] A. van Houselt, R. van Gastel, B. Poelsema, and H. J. W. Zandvliet, Phys. Rev. Lett. **97**, 266104 (2006).

[36] T. Sato, M. Iwatsuki, and H. Tochihara, J. Electron Microsc. **48**, 1 (1999).

[37] M. Kubota and Y. Murata, Phys. Rev. B **49**, 4810 (1994).

[38] A. Compaan, M. C. Lee, and G. J. Trott, Phys. Rev. B **32**, 6731 (1985).